## PROCEEDINGS OF SPIE

SPIEDigitalLibrary.org/conference-proceedings-of-spie

# Comparing the polarimetric response of hyperspectral imagers

Logan, Riley, Venkatesulu, Erica, Shaw, Joseph

Riley D. Logan, Erica Venkatesulu, Joseph A. Shaw, "Comparing the polarimetric response of hyperspectral imagers," Proc. SPIE 11833, Polarization Science and Remote Sensing X, 118330H (1 August 2021); doi: 10.1117/12.2595588



Event: SPIE Optical Engineering + Applications, 2021, San Diego, California, United States

### Comparing the polarimetric response of hyperspectral imagers

Riley D. Logan<sup>a</sup>, Erica Venkatesulu<sup>a</sup>, and Joseph A. Shaw<sup>a</sup>

<sup>a</sup>Electrical and Computer Engineering Department, Montana State University, P.O. Box 173780, Bozeman, USA

#### **ABSTRACT**

Optical remote sensing systems are often used to gather imagery of scenes containing partially polarized light. Partially polarized reflection or emission will affect the detected response if the sensor system has intentional or unintentional polarization sensitivity. As the use of optical remote sensing systems becomes more widespread, the factors affecting the response of these systems needs to be better understood. In this paper, we present the results of polarization response measurements of six hyperspectral imaging systems manufactured by Resonon Inc. The imagers included in this study cover wavelengths from approximately 350 nm to 1700 nm, with various spectral sampling rates. Efforts are ongoing to model and compensate for the observed response.

Keywords: Remote Sensing, Polarization, Polarimetry, Radiometry, Hyperspectral Imaging

#### 1. INTRODUCTION

Hyperspectral imaging is being applied more widely in remote sensing, owing to the rich spectral and spatial information content.<sup>1</sup> Similarly, polarization imaging is being used increasingly often to provide information beyond what is available from intensity and color alone.<sup>2</sup> These modalities have been purposefully combined to create polarimetric hyperspectral imagers<sup>3,4</sup> for remote sensing applications that include material characterization,<sup>5</sup> ocean color and aerosol sensing,<sup>6–11</sup> and enhanced underwater imaging.<sup>12</sup> Partially polarized scenes cause measurement errors when conventional multispectral and hyperspectral imaging systems not designed for polarimetry have unintentional polarization sensitivity.<sup>13–17</sup> For example, a drone-mounted hyperspectral imager that we use for detecting river algae has a weak, spectrally variable polarization sensitivity that can cause errors when viewing partially polarized river scenes or when used with a polarizer to suppress water surface reflections.<sup>18</sup>

Although hyperspectral imagers are commonly used to analyze scenes which contain partially polarized light, few studies have been conducted to analyze the polarization response of these systems. In this paper, we build on previous work in analyzing our drone-based hyperspectral imager<sup>18</sup> and extend our analysis to a wider variety of hyperspectral imaging systems manufactured by our collaborating company, Resonon Inc, with spectral ranges varying from 350 nm to 1700 nm. We restrict our discussion to linearly polarized light.

#### 2. EXPERIMENTAL METHODS

The goal of our analysis was to determine the polarization response of several grating-based hyperspectral imaging systems manufactured by Resonon, Inc. Each of the imaging systems tested were loaned to us based on availability, though a wide range of imagers were tested (Table 1). We used an integrating sphere (Labsphere USLR-V12F-NDNN) and a 129-mm-diameter wire-grid polarizer with an extinction ratio of at least 1000 between 400 nm to 1000 nm (Meadowlark Optics VLM-129-UV-C) to generate the linear polarization states required to analyze the polarimetric response of the imagers. The integrating sphere provided spatially uniform, randomly polarized light that we directed through the wire-grid polarizer mounted in a rotation stage, resulting in a user-controlled linearly polarized signal. We placed each of the hyperspectral imagers on a rotation stage mounted on a tripod and directed the imager to view the light transmitted through the wire-grid

Further author information: (Send correspondence to Dr. Joseph A. Shaw) Joseph A. Shaw: E-mail: joseph.shaw@montana.edu, Telephone: +1 406-994-7261

Polarization Science and Remote Sensing X, edited by Meredith K. Kupinski, Joseph A. Shaw, Frans Snik, Proceedings of SPIE Vol. 11833, 118330H ⋅ © 2021 SPIE CCC code: 0277-786X/21/\$21 ⋅ doi: 10.1117/12.2595588

polarizer, as depicted in Figure 1. Each imager was scanned through an angular range of approximately  $5^{\circ}$  centered on normal incidence, meaning the maximum incidence angle between the surface of the polarizer and the imager was approximately  $\pm 2.5^{\circ}$ . Each imager was controlled using the SpectrononPro software package with gain = 1 and other settings outlined in Table 1.

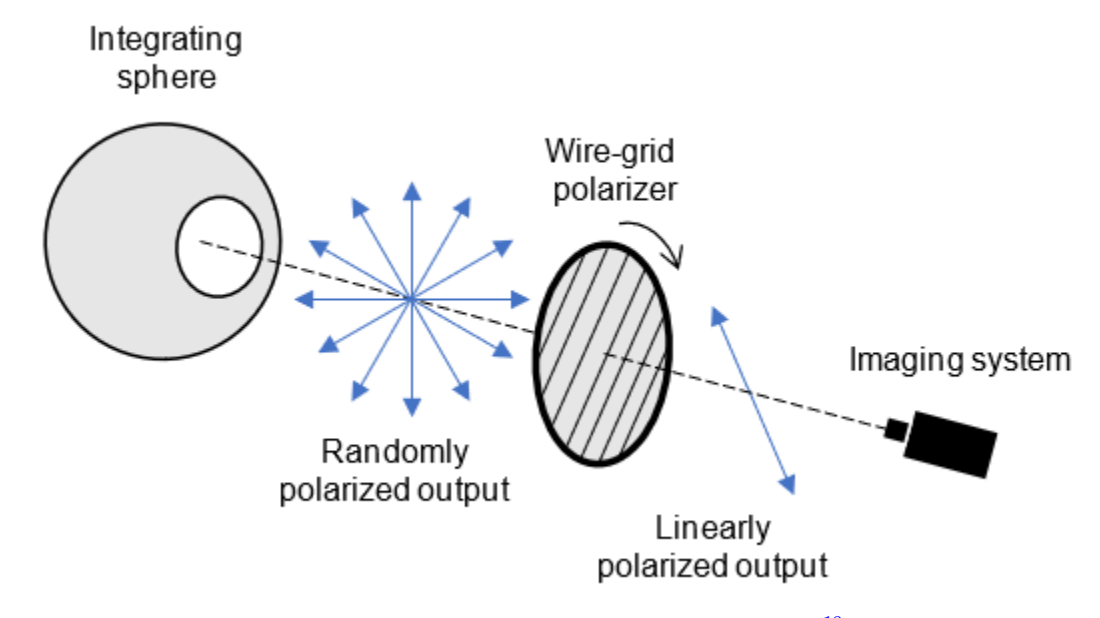


Figure 1. Experimental setup showing our light source, wire-grid polarizer, and imager. <sup>18</sup> Note that linearly polarized light is transmitted through the wire-grid in a state orthogonal to the wire grid.

| Table 1. Hyperspectral | imaging systems an | alyzed and imager | settings (gain = 1 | for all imagers). |
|------------------------|--------------------|-------------------|--------------------|-------------------|
|                        |                    |                   |                    |                   |

| Imager      | Spectral Range [nm] | Spectral Sampling [nm] | Integration Time [ms] | Frame Rate [fps] |
|-------------|---------------------|------------------------|-----------------------|------------------|
| Pika NUV    | 350 - 850           | 1.9                    | 32                    | 30               |
| Pika XC2    | 400 - 1000          | 1.3                    | 10                    | 90               |
| Pika L      | 400 - 1000          | 2.1                    | 10                    | 30               |
| Pika NIRC   | 900 - 1700          | 3.3                    | 6                     | 30               |
| Pika NIR320 | 900 - 1700          | 4.9                    | 15                    | 29.77            |

To ensure no stray light entered the system, we gathered images in a dark, light-tight room with baffling in the path between the imager and polarizer. As an additional precaution against stray light, we shrouded the full experimental setup. We began with the wire-grid polarizer oriented to pass vertically polarized light (0°), then rotated the polarizer clockwise, as viewed from the imager, in steps of  $2^{\circ}$  for  $180^{\circ}$ , then  $6^{\circ}$  for an additional  $180^{\circ}$ . Four hyperspectral data cubes were captured at each polarizer angle and averaged to reduce random noise. After averaging, we applied a radiometric calibration on the data cubes to remove any wavelength-dependent response introduced by the imaging system. We performed all of our radiometric calibrations using calibration files provided by Resonon Inc, which related digital number to spectral radiance for each imager. Once we calibrated each data cube, we analyzed the polarization response of each imager by relating the change in spectral radiance as a function of polarizer angle. Additionally, we calculated the apparent  $S_0$ ,  $S_1$ , and  $S_2$  Stokes parameters and the apparent degree of linear polarization (DoLP) that expressed the polarization sensitivity for each imager.

#### 3. RESULTS AND DISCUSSION

To determine the polarization response of the hyperspectral imaging systems, we began by calculating the linear Stokes parameters as

$$S_0 = L_{0^{\circ}} + L_{90^{\circ}} \tag{1}$$

$$S_1 = L_{0^{\circ}} - L_{90^{\circ}} \tag{2}$$

$$S_2 = L_{45^{\circ}} - L_{135^{\circ}}, \tag{3}$$

where  $L_{0^{\circ}}$ ,  $L_{90^{\circ}}$ ,  $L_{45^{\circ}}$ , and  $L_{135^{\circ}}$  represent the detected spectral radiance for vertically, horizontally,  $45^{\circ}$ , and  $135^{\circ}$  polarized light, respectively. Once the three linear Stokes parameters were determined for each imager, we calculated the apparent degree of linear polarization (DoLP) as

$$DoLP = \frac{\sqrt{S_1^2 + S_2^2}}{S_0}. (4)$$

Calculation of the DoLP is common when analyzing the decimal fraction of an electromagnetic wave that is linearly polarized; however, we use the DoLP to represent the variation in the measured signal introduced by polarizer angle. That is, if the imaging system had no polarization response, we would expect it to follow Malus' Law and record a value of  $S_0/2$  for all polarizer angles. Here, we used the DoLP to show the amount by which the recorded signal extended above and below  $S_0/2$ . To visualize this quantity, we calculated the DoLP as a function of wavelength for each of the imagers. Our previous polarization response measurements of the Resonon Pika L system showed a clear dependence on the polarization state of the input light, with the maximum response in the near-infrared wavelengths (Fig. 2). The new polarization response measurements are shown in Figures 3, 4, 5, 6, and 7. Figure 2 shows our previous DoLP measurements of our Pika L imaging system, whereas Figure 3 shows new DoLP measurements of a different Pika L system loaned to us from Resonon Inc. The two measurements of DoLP show significant similarity, with our previous measurements showing a peak DoLP of approximately 0.073 (7.3%) at 744 nm and measurements of the loaned imager showing a peak DoLP of 0.059 (5.9%) at 733 nm. The DoLP spectral dependence shows a similar pattern for both imagers, with the DoLP varying within the range of 0 to 0.07.

The DoLP calculated for the imagers included in this work reveal a strong dependence on wavelength. The spectral locations and minimum and maximum DoLP calculated for each imaging system are shown in Table 2.

| Imager      | Spectral Range [nm] | DoLP (max) | Wavelength [nm] | DoLP (min) | Wavelength [nm] |
|-------------|---------------------|------------|-----------------|------------|-----------------|
| Pika NUV    | 350 - 850           | 0.135      | 609             | 0.007      | 351             |
| Pika XC2    | 400 - 1000          | 0.101      | 850             | 0.004      | 593             |
| Pika L      | 400 - 1000          | 0.059      | 733             | 0.0003     | 542             |
| Pika NIRC   | 900 - 1700          | 0.019      | 1251            | 0.004      | 1045            |
| Pika NIR320 | 900 - 1700          | 0.114      | 1505            | 0.009      | 1294            |

Table 2. Spectral locations of minimum and maximum DoLP values.

The result presented in Table 2 show that, if unaccounted for, polarized light will result in maximum errors ranging from 13.5% at 609 nm for the Pika NUV system to 1.9% at 1251 nm for the Pika NIRC system. The minimum polarization sensitivity was less than 1% for all imagers tested.

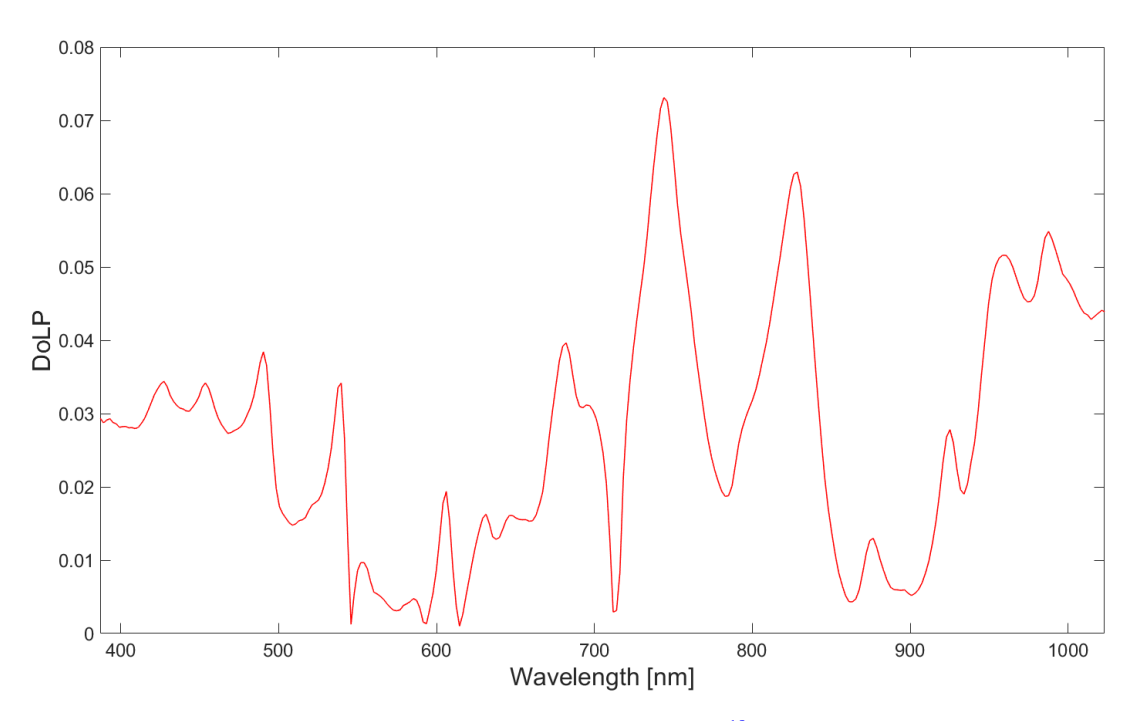


Figure 2. Previous DoLP measurements of our Pika L hyperspectral imager. <sup>18</sup> Measurements are shown across full spectral range of imager.

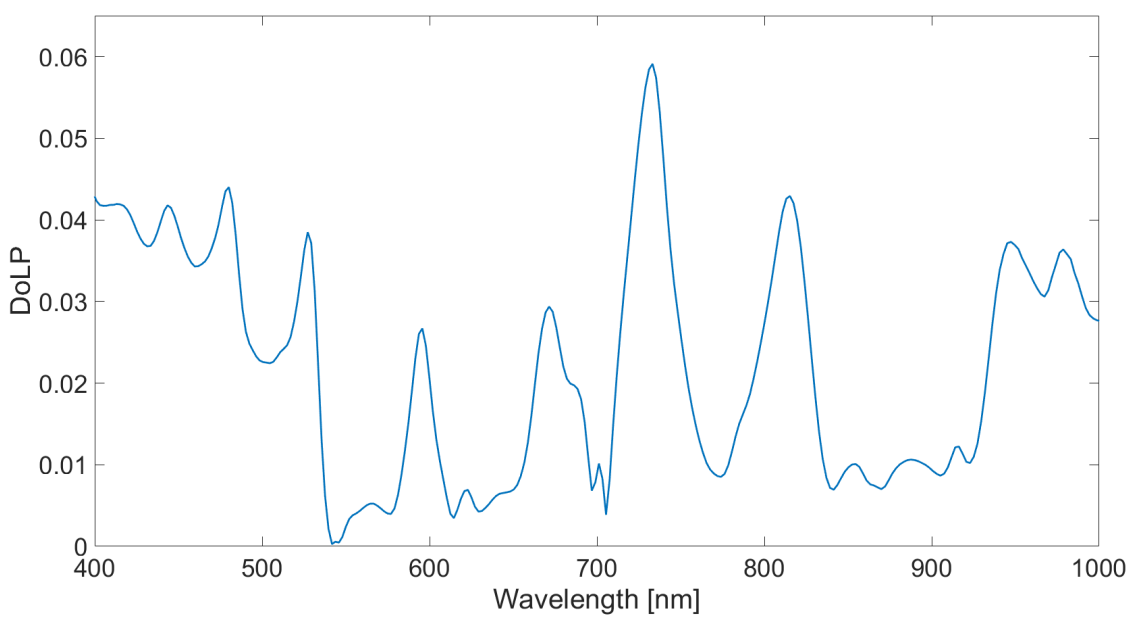


Figure 3. DoLP measurements of loaned Pika L hyperspectral imager. Measurements are shown across full spectral range of imager.

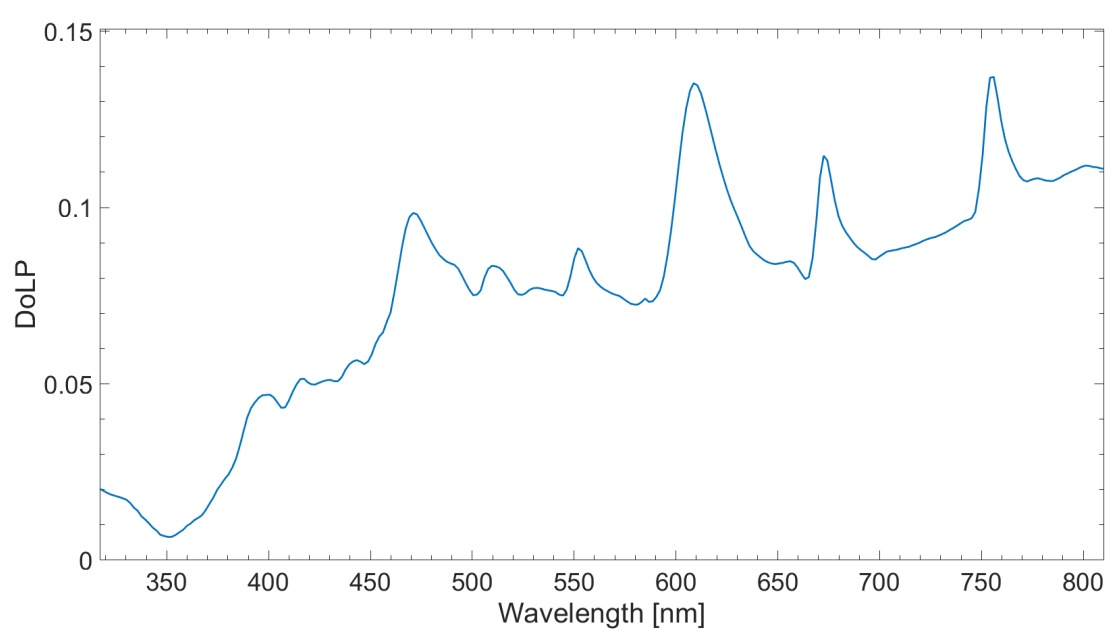


Figure 4. DoLP measurements of the Pika NUV hyperspectral imaging system. Measurements are shown across full spectral range of the imager.

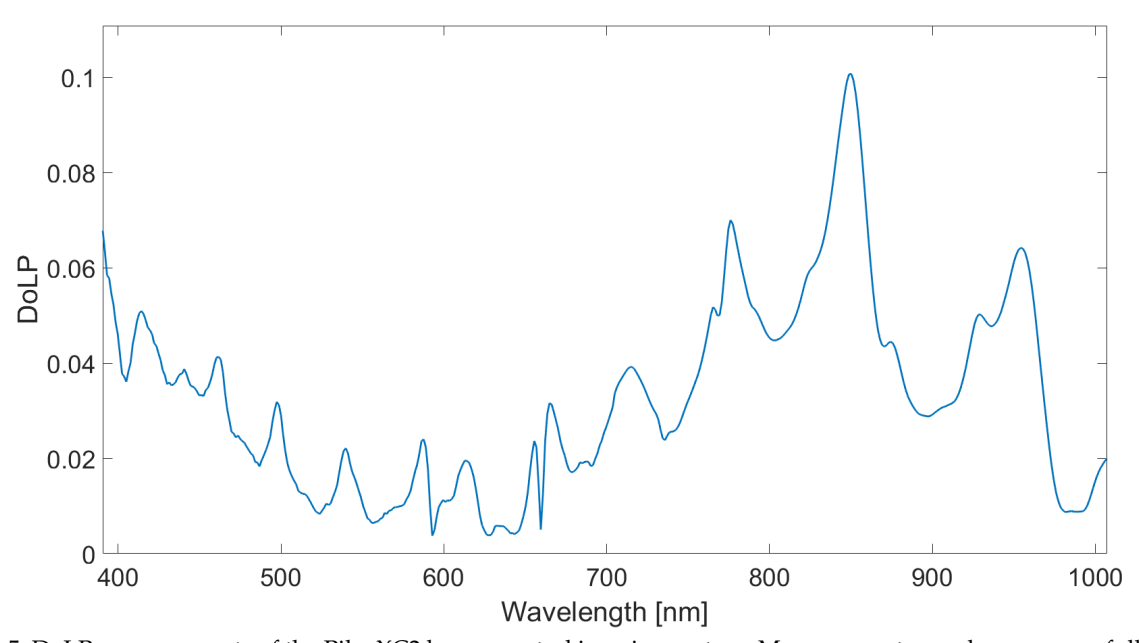


Figure 5. DoLP measurements of the Pika XC2 hyperspectral imaging system. Measurements are shown across full spectral range of the imager.

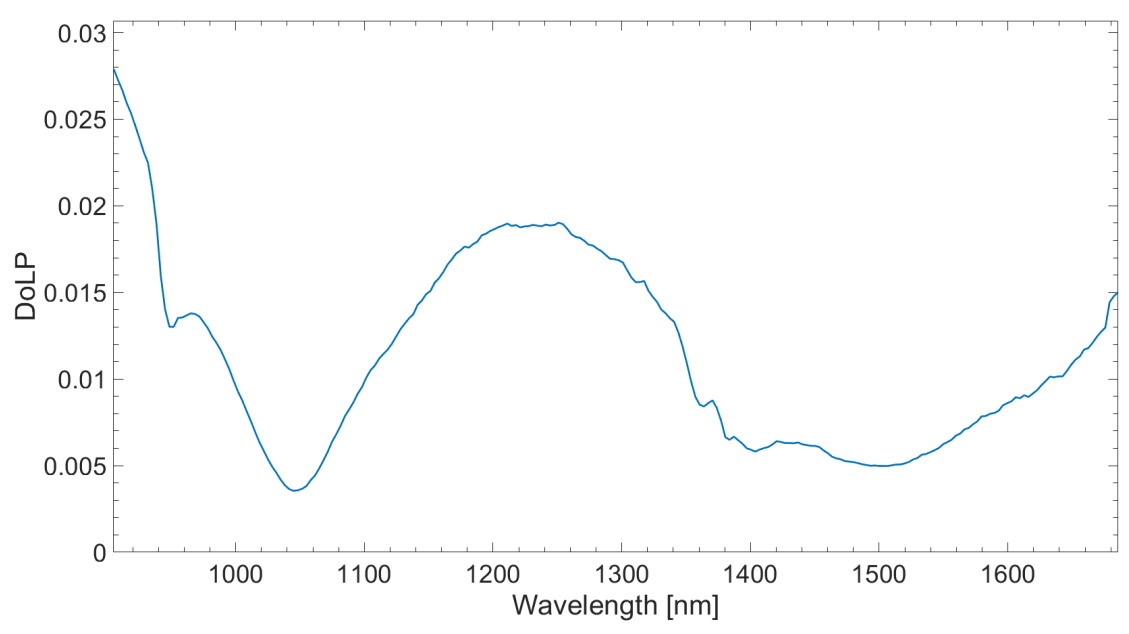


Figure 6. DoLP measurements of the Pika NIRC hyperspectral imaging system. Measurements are shown across full spectral range of the imager.

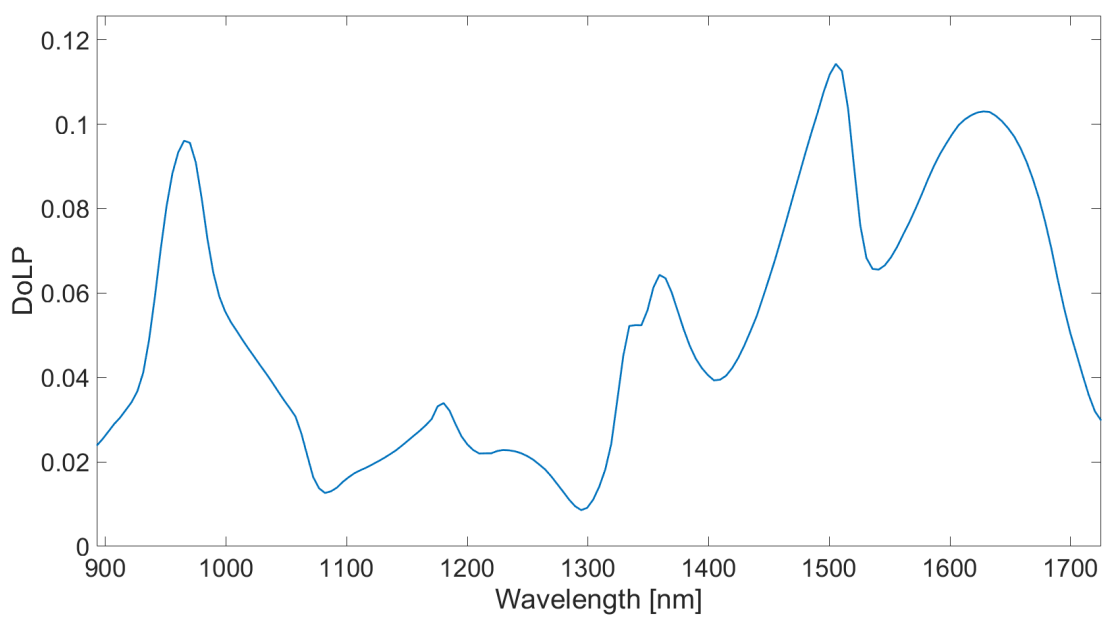


Figure 7. DoLP measurements of the Pika NIR320 hyperspectral imaging system. Measurements are shown across full spectral range of the imager.

#### 4. CONCLUSION

As the use of optical remote sensing systems becomes more widespread, the need for calibration becomes more important. Often, remote sensing systems are calibrated radiometrically, without accounting for polarization sensitivity. Here we presented the results of polarization response measurements of six grating-based hyperspectral imaging systems manufactured by Resonon Inc.

To measure the polarization response of each imaging system, we first generated a 100% linearly polarized signal using an integrating sphere and a wire-grid polarizer mounted in a rotation stage. We then directed each imager to collect the light transmitted through the wire-grid polarizer, with baffling in place to reduce the effects of stray light entering the system. To generate the required linear polarization states, we rotated the polarizer through 360° in variable step sizes and captured imagery at each degree step. From the captured imager, we calculated the linear Stokes parameters and the apparent DoLP. The DoLP showed a strong dependence on wavelength for each imaging system, with maximum errors ranging from 13.5% at 609 nm for the Pika NUV system to 1.9% at 1251 nm for the Pika NIRC system. The minimum polarization sensitivity was less than 1% for all imagers tested.

Efforts are ongoing to model the polarization effects of the diffraction grating in each of the imaging systems and to compensate for the observed polarization response. Correction of the observed polarization response would allow the imagers analyzed to collect more accurate measurements when gathering data that contain polarized signals.

#### **ACKNOWLEDGMENTS**

This material is based upon work supported in part by the National Science Foundation EPSCoR Cooperative Agreement OIA-1757351. Any opinions, findings, and conclusions or recommendations expressed in this material are those of the author(s) and do not necessarily reflect the views of the National Science Foundation.

#### REFERENCES

- [1] Eismann, M. T., [Hyperspectral Remote Sensing], SPIE (2012).
- [2] Tyo, J. S., Goldstein, D. L., Chenault, D. B., and Shaw, J. A., "Review of passive imaging polarimetry for remote sensing applications," *Applied Optics* **45**(22), 5453–5469 (2006).
- [3] Craven-Jones, J., Kudenov, M. W., Stapelbroek, M. G., and Dereniak, E. L., "Infrared hyperspectral imaging polarimeter using birefringent prisms," *Appl. Opt.* **50**, 1170–1185 (Mar 2011).
- [4] Mu, T., Zhang, C., Jia, C., and Ren, W., "Static hyperspectral imaging polarimeter for full linear stokes parameters," *Opt. Express* **20**, 18194–18201 (Jul 2012).
- [5] Martin, J. A. and Gross, K. C., "Estimating index of refraction from polarimetric hyperspectral imaging measurements," *Opt. Express* **24**, 17928–17940 (Aug 2016).
- [6] Shaw, J., "Degree of linear polarization in spectral radiances from water-viewing infrared radiometers.," *Applied optics* **38 15**, 3157–65 (1999).
- [7] Jr., F. J. I., Shaw, J. A., Jones, S. H., and Scott, H. E., "Snapshot LWIR hyperspectral polarimetric imager for ocean surface sensing," in [*Polarization Analysis, Measurement, and Remote Sensing III*], Chenault, D. B., Duggin, M. J., Egan, W. G., Goldstein, D. H., Egan, W. G., and Duggin, M. J., eds., **4133**, 270 283, International Society for Optics and Photonics, SPIE (2000).
- [8] Shaw, J. A., "Polarimetric measurements of long-wave infrared spectral radiance from water," *Appl. Opt.* **40**, 5985–5990 (Nov 2001).
- [9] Gao, M., Zhai, P.-W., Franz, B. A., Knobelspiesse, K., Ibrahim, A., Cairns, B., Craig, S. E., Fu, G., Hasekamp, O., Hu, Y., and Werdell, P. J., "Inversion of multiangular polarimetric measurements from the acepol campaign: an application of improving aerosol property and hyperspectral ocean color retrievals," *Atmospheric Measurement Techniques* **13**(7), 3939–3956 (2020).
- [10] Gilerson, A., Carrizo, C., Ibrahim, A., Foster, R., Harmel, T., El-Habashi, A., Lee, Z., Yu, X., Ladner, S., and Ondrusek, M., "Hyperspectral polarimetric imaging of the water surface and retrieval of water optical parameters from multi-angular polarimetric data," *Appl. Opt.* **59**, C8–C20 (Apr 2020).

- [11] Hannadige, N. K., Zhai, P.-W., Gao, M., Franz, B. A., Hu, Y., Knobelspiesse, K., Werdell, P. J., Ibrahim, A., Cairns, B., and Hasekamp, O. P., "Atmospheric correction over the ocean for hyperspectral radiometers using multi-angle polarimetric retrievals," *Opt. Express* **29**, 4504–4522 (Feb 2021).
- [12] Schechner, Y. and Karpel, N., "Recovery of underwater visibility and structure by polarization analysis," *IEEE Journal of Oceanic Engineering* **30**(3), 570–587 (2005).
- [13] Shaw, J. A., "The effect of instrument polarization sensitivity on sea surface remote sensing with infrared spectroradiometers," *Journal of Atmospheric and OCeanic Technology* **19**, 820–827 (May 2002).
- [14] Pagano, T. S., Aumann, H. H., Elliott, D., and Broberg, S. E., "AIRS infrared polarization sensitivity and in-flight observations," in [*Earth Observing Systems IX*], Barnes, W. L. and Butler, J. J., eds., **5542**, 45 52, International Society for Optics and Photonics, SPIE (2004).
- [15] Sun, J.-Q. and Xiong, X., "Modis polarization-sensitivity analysis," *IEEE Transactions on Geoscience and Remote Sensing* **45**(9), 2875–2885 (2007).
- [16] Taylor, J. K., Revercomb, H. E., and Tobin, D. C., "An analysis and correction of polarization induced calibration errors for the cross-track infrared sounder (cris) sensor," in [Light, Energy and the Environment 2018 (E2, FTS, HISE, SOLAR, SSL)], Light, Energy and the Environment 2018 (E2, FTS, HISE, SOLAR, SSL), FW2B.3, Optical Society of America (2018).
- [17] Angal, A., Geng, X., Xiong, X., Twedt, K., Wu, A., Link, D., and Aldoretta, E., "On-orbit calibration of terra modis vis bands using polarization-corrected desert observations," *IEEE Transactions on Geoscience and Remote Sensing* **58**, 5428–5439 (2020).
- [18] Logan, R. D. and Shaw, J. A., "Measuring the polarization response of a VNIR hyperspectral imager," in [Polarization: Measurement, Analysis, and Remote Sensing XIV], Chenault, D. B. and Goldstein, D. H., eds., 11412, 113 119, International Society for Optics and Photonics, SPIE (2020).